



Contents lists available at ScienceDirect

Computers and Structures

journal homepage: www.elsevier.com/locate/compstruc

Inf-sup testing of some three-dimensional low-order finite elements for the analysis of solids

Yeongbin Ko^a, Klaus-Jürgen Bathe^{b,*}

^a ADINA R & D, Inc., 71 Elton Ave, Watertown, MA 02472, USA

^b Department of Mechanical Engineering, Massachusetts Institute of Technology, Cambridge, MA 02139, USA

ARTICLE INFO

Article history:

Received 12 May 2018

Accepted 27 July 2018

Available online xxxxx

Keywords:

Stability and accuracy of finite element solutions

Inf-sup tests

Volumetric locking

Shear locking

Membrane locking, pinching locking

ABSTRACT

We assess some 8-node hexahedral three-dimensional (3D) solid elements using inf-sup tests focusing on locking behavior in volumetric, shear, membrane, and pinching actions. Inf-sup tests have been widely used to see whether a finite element discretization is effective. In this paper we use a rather simple approach to inf-sup testing for the coercivity of the discretization to obtain insight into the convergence behavior of the standard displacement-based element, the 8-node element with incompatible modes, and the 3D-MITC8 element, and include geometric nonlinear analysis. We see that the 3D-MITC8 element performs better than the incompatible modes element in plate bending problems and can also be used with a small modification in the solution of thick or moderately thick curved shell structures.

© 2018 Elsevier Ltd. All rights reserved.

1. Introduction

Finite element methods are now abundantly used to solve three-dimensional (3D) elasticity problems. An 8-node hexahedral element is widely used for modeling and analysis of 3D solids. However, the standard 8-node displacement-based element suffers from severe loss of accuracy caused by locking. Ideally, a finite element solution should be stable and the solution error should decrease optimally regardless of the problem type considered, including the analysis of incompressible media and the analysis of bending, membrane and mixed behaviors of plate and shell structures [1,2].

The stability and accuracy of finite element solutions can be assessed by investigating whether the ellipticity, continuity and relevant inf-sup conditions are satisfied [1–4]. These conditions give requirements on the interpolations used in an element formulation. If a finite element scheme is consistent and the basic requirements of ellipticity, continuity and the inf-conditions are satisfied, optimal error bounds can be established and hence the uniform accuracy of a finite element scheme is guaranteed [1–4]. However, proving analytically that the conditions are satisfied for an element used in the analysis of incompressible media and plate and shell structures can be extremely difficult.

To obtain insight into an element formulation, it is valuable to employ the numerical ‘inf-sup test’ proposed by Chapelle and Bathe [5]. This test and variations thereof have been widely used for different finite element formulations of physical problems, including to assess finite formulations for the analysis of solids, plates and shells, and fluid flows, see for example Refs. [6–9] for some early use and Refs. [10–14] for some recent use.

In this paper, we use inf-sup tests to obtain more insight into the recently proposed 8-node hexahedral element, the 3D-MITC8 element [15], and compare the results with those obtained for the standard 8-node displacement-based (H8) element [1] and the element with incompatible modes, the H8I9 element [16]. The formulation of the 3D-MITC8 element is based on the MITC method to alleviate volumetric and shear locking, and with a small modification can also be used for the analysis of shell structures. While various problem solutions have already been presented in Ref. [15], further insight into the behavior of the element is of significant interest.

In previous research using inf-sup tests, specific locking conditions have been focused on. The locking in the solution of incompressible media was for example considered in Ref. [5], shear locking in plate analyses was considered in Ref. [17], locking in the bending analysis of shells was studied in Ref. [18], and pinching locking was investigated in Ref. [19]. These tests require the use of the mixed formulation of the finite element discretization with the constraint equations explicitly given in the formulation. However, for the 3D-MITC8 element, we do not have the constraint equa-

* Corresponding author.

E-mail address: kjb@mit.edu (K.J. Bathe).

tions explicitly – instead we have a displacement formulation with the constraints embedded in the formulation [20]. Hence the inf-sup condition that we use to test the elements is written in terms of the displacement degrees of freedom only and we test for coercivity with the aim to obtain at the same time also insight into the locking behavior of the elements when used in the solutions of different physical problems.

In the subsequent sections, we briefly review some fundamental equations for an effective finite element discretization for the linear analysis of incompressible media, plate and shell structures. For the analysis of curved shells we propose the 3D-MITC8/s element reached by a small modification of the formulation of the 3D-MITC8 element. We then perform numerical inf-sup testing to investigate the performance of the H8, H8I9, 3D-MITC8 and 3D-MITC8/s elements. We also apply the inf-sup test to obtain insight into the instability seen in the incompatible modes element when used in geometric nonlinear analysis.

2. The inf-sup condition

In this section we present the inf-sup equation that we use to study the behavior of the elements in the various problem solutions that we consider. We also use the inf-sup test to obtain insight into the effectiveness of the finite elements in a nonlinear analysis.

2.1. The inf-sup conditions in linear analysis

We consider the structural domain Ω in Fig. 1(a). The displacement boundary conditions and the vector \mathbf{f} of external forces are applied over the surfaces S_U and S_f and volume Ω respectively. The elasticity problem of the continuum can be stated as [1];

$$\forall \mathbf{w} \text{ find } \mathbf{v} \text{ such that } a(\mathbf{w}, \mathbf{v}) = (\mathbf{f}, \mathbf{w}),$$

$$a(\mathbf{w}, \mathbf{v}) = 2G \int_{\Omega} e_{ij}^{dev}(\mathbf{w})e_{ij}^{dev}(\mathbf{v})d\Omega + \kappa \int_{\Omega} e^{vol}(\mathbf{w})e^{vol}(\mathbf{v})d\Omega,$$

$$e^{vol} = e_{xx} + e_{yy} + e_{zz}, \quad e_{ij}^{dev} = e_{ij} - \frac{1}{3}e^{vol}\delta_{ij},$$

$$G = \frac{E}{2(1+\nu)} \text{ and } \kappa = \frac{E}{3(1-2\nu)},$$

in which $a(\cdot, \cdot)$ and (\mathbf{f}, \cdot) are bilinear and linear forms, e_{ij} are the strain components in the global Cartesian coordinates $x_1 = x,$

$x_2 = y, x_3 = z, E$ and ν are Young’s modulus and Poisson’s ratio, respectively, and G and κ are the shear and bulk moduli. Here $e_{11} = e_{xx}, e_{22} = e_{yy}, e_{33} = e_{zz}, e_{12} = e_{xy}, e_{23} = e_{yz}$ and $e_{31} = e_{zx}.$

In Eq. (1), the solution \mathbf{v} and test function \mathbf{w} are elements of the space

$$V = \left\{ \mathbf{v} \in \mathbb{R}^3 \mid \mathbf{v} \in L^2(\Omega), \frac{\partial v_i}{\partial x_j} \in L^2(\Omega), v_i|_{S_U} = 0 \text{ with } i, j = 1, 2, 3 \right\},$$

(2)

in which we use the notation $v_1 = v_x, v_2 = v_y, v_3 = v_z$ to denote the components of \mathbf{v} in the global Cartesian coordinate directions. The natural norm used with this space is the H^1 norm. The external force is an element in the dual space V^* corresponding to $V.$

We use the 3D finite elements of domains $\Omega_h^{(k)}$ and size h to discretize the continuum so that

$$\bigcup_k \Omega_h^{(k)} = \Omega_h \rightarrow \Omega \text{ as } h \rightarrow 0.$$

(3)

The finite element problem with the discretization is then given by [1]

$$\forall \mathbf{w}_h \text{ find } \mathbf{v}_h \text{ such that } \mathbf{w}_h^T \mathbf{A}_h \mathbf{v}_h = \mathbf{w}_h^T \mathbf{F}_h,$$

(4)

where \mathbf{A}_h is the stiffness matrix, \mathbf{F}_h is the vector of externally applied forces, the solution vector is $\mathbf{v}_h \in V_h$ with also $\mathbf{w}_h \in V_h$ corresponding to \mathbf{v} and \mathbf{w} , respectively, and the solution space $V_h \subset V$ is

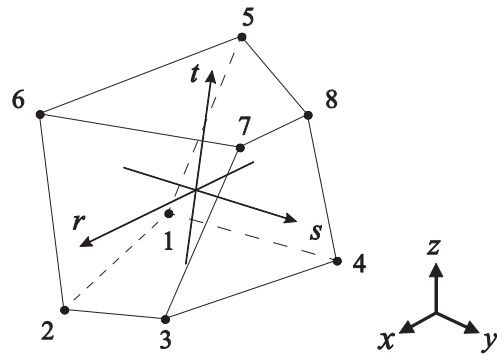


Fig. 2. A standard 8-node hexahedral 3D solid element.

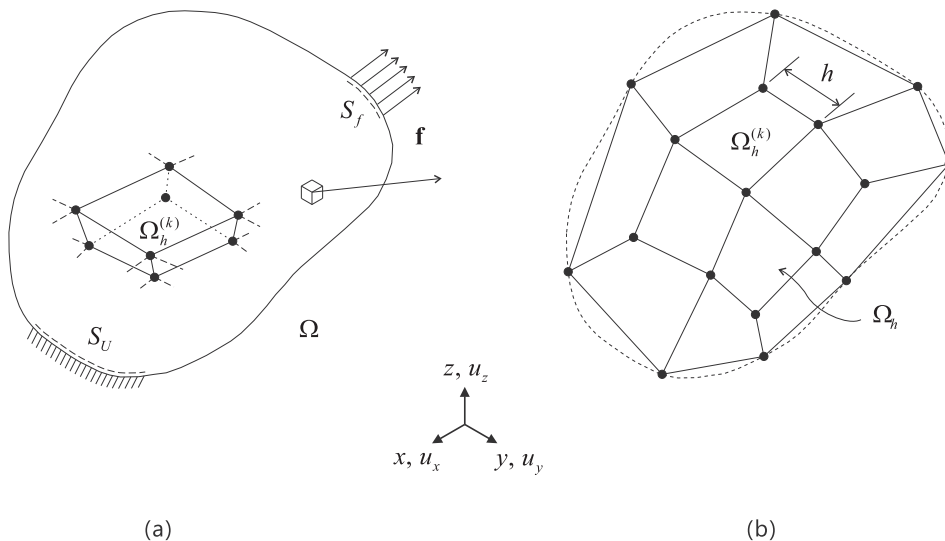


Fig. 1. 3D elasticity problem. (a) Continuum with one finite element shown. (b) Discrete domain.

$$V_h = \left\{ \mathbf{v}_h \in \mathbb{R}^3 \mid \mathbf{v}_h \in L^2(\Omega_h), \frac{\partial(v_h)_i}{\partial x_j} \in L^2(\Omega_h), (v_h)_i|_{S_U} = 0 \text{ with } i,j=1,2,3 \right\}. \quad (5)$$

Here \mathbf{F}_h is an element of the dual space V_h^* corresponding to V_h .

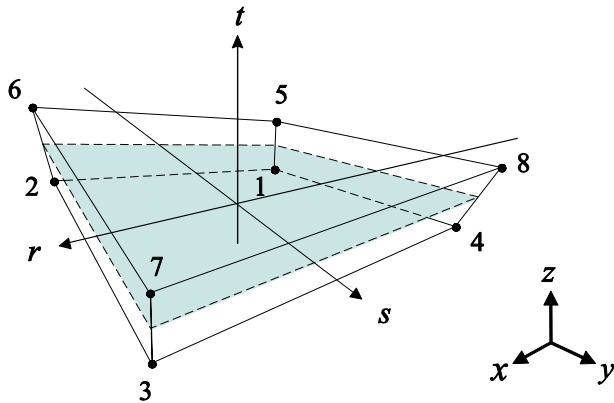


Fig. 3. An 8-node element with its mid-surface at $t = 0$.

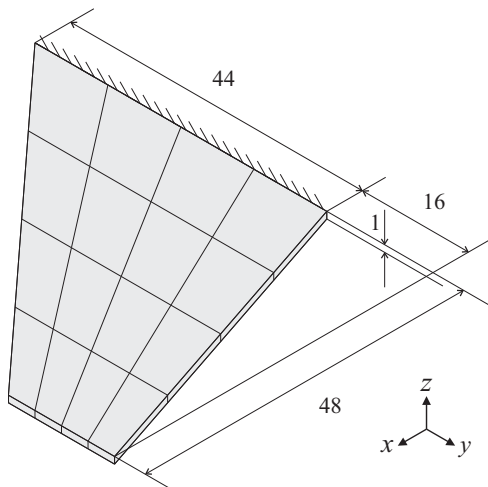


Fig. 4. Cook's cantilever (plane strain conditions, $E = 1.0$, and $\nu = 0.3, 0.4$ or 0.499). The mesh of 4×4 elements is shown.

We denote by $\|\cdot\|$ and $\|\cdot\|_*$ the norm and dual norm used to measure the size of the finite element solution $\mathbf{v}_h \in V_h$ and external force vector $\mathbf{F}_h \in V_h^*$. The dual norm is given by

$$\|\mathbf{F}_h\|_* = \sup_{\mathbf{w}_h \in V_h} \frac{\mathbf{w}_h^T \mathbf{F}_h}{\|\mathbf{w}_h\|}. \quad (6)$$

To have a stable solution we need that a small change in the load vector $\Delta \mathbf{F}_h$ should yield only a small change in the solution vector $\Delta \mathbf{x}_h$. Hence considering $\mathbf{A}_h \Delta \mathbf{x}_h = \Delta \mathbf{F}_h$ and $\mathbf{A}_h \mathbf{x}_h = \mathbf{F}_h$ we define the following stability constant (S)

$$\frac{\|\Delta \mathbf{x}_h\|}{\|\mathbf{x}_h\|} \leq S \frac{\|\Delta \mathbf{F}_h\|_*}{\|\mathbf{F}_h\|_*}, \quad (7)$$

where S should remain bounded regardless of the mesh used, that is, for all mesh sequences when $h \rightarrow 0$. It can be shown that a condition is [1–4]

$\exists \gamma_A > 0$ independent of h such that

$$\inf_{\mathbf{w}_h \in V_h} \sup_{\mathbf{v}_h \in V_h} \frac{\mathbf{w}_h^T \mathbf{A}_h \mathbf{v}_h}{\|\mathbf{w}_h\| \|\mathbf{v}_h\|} \geq \gamma_A, \quad (8)$$

which is the inf-sup condition for the matrix \mathbf{A}_h . We will focus on this condition in our assessment of the elements.

In earlier inf-sup testing, the mixed finite element formulation was explicitly given and focused on. However, in this paper we simply use Eq. (8) for displacement degrees of freedom only and evaluate this condition numerically in the analysis of incompressible media, plates and shells by the selection of specific geometric domains with specific boundary and material conditions. Hence we in fact focus on the coercivity of the discretization as the mesh is refined with the aim to also identify whether the discretization (that is, the element used) is locking [20].

2.2. Inf-sup condition in nonlinear analysis

In the above equations we assumed, as is usually done, linear analysis conditions. However we can also include geometric nonlinearities, in which case we use the following $\hat{\mathbf{A}}_h$ in place of \mathbf{A}_h in Eq. (8),

$$\hat{\mathbf{A}}_h = \mathbf{A}_h + \mathbf{S}_h, \quad (9)$$

where we have, without focusing on details,

$$\mathbf{w}_h^T \mathbf{S}_h \mathbf{v}_h = \sum_k \int_{\Omega_h^{(k)}} \tau_{ij} \delta \eta_{ij}(\mathbf{w}_h, \mathbf{v}_h) d\Omega_h^{(k)}, \quad (10)$$

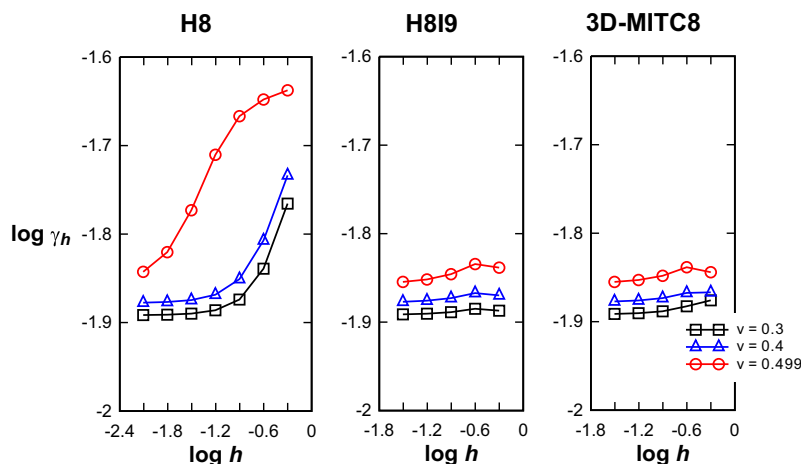


Fig. 5. Inf-sup convergence curves for Cook's cantilever.

where we sum over all elements and τ_{ij} is the internal stress at the configuration considered and $\delta\eta_{ij}$ is the variation of the nonlinear part of the Green–Lagrange strain, for details see for example Ref. [1]. The matrix $\widehat{\mathbf{A}}_h$ is the tangent stiffness matrix in geometric nonlinear analysis in the current configuration.

The tangent stiffness matrix is not always positive definite. The matrix positive definiteness can be lost in geometric or material nonlinear analyses due to the physical conditions modeled [1]. However, a different instability phenomenon occurs for certain element formulations which is spurious and purely numerical, indicating an unreliable element formulation unless some remedy is used [21–23]. This instability was first noticed in large strain analyses but was then also identified to occur in large displacement but small strain conditions [24].

Denoting by ε_{ij} the global Cartesian components of the element initial strain, Sussman and Bathe [24] showed that a spurious mechanism renders the tangent stiffness matrix of the H819 element indefinite at the following critical limit in volumetric strain

$$\varepsilon^{vol} = \varepsilon_{crit} = -\left(\frac{L_2}{L_1}\right)^2, \tag{11}$$

$$\varepsilon^{vol} = \varepsilon_{xx} + \varepsilon_{yy} + \varepsilon_{zz},$$

where L_1 and L_2 give the length and width of the in-plane rectangular element ($L_1 > L_2$). The initial stress is obtained as $\tau_{ij} = \varepsilon^{vol} + 2G\varepsilon_{ij}^{dev}$ with $\varepsilon_{ij}^{dev} = \varepsilon_{ij} - \frac{1}{3}\varepsilon^{vol}\delta_{ij}$. This condition can clearly be reached in small strain situations.

2.3. Evaluation of inf-sup expressions and inf-sup testing

For the solutions $\mathbf{v}_h \in V_h$, we use the H^1 norm for the discretization [1,2]

$$\|\mathbf{v}_h\| = \left(\sum_k \int_{\Omega_h^{(k)}} \left[(v_h)_i^2 + \left(\frac{\partial(v_h)_i}{\partial x_j} \right)^2 \right] d\Omega_h^{(k)} \right)^{1/2} = \sqrt{\mathbf{v}_h^T \mathbf{G}_h \mathbf{v}_h}, \tag{12}$$

where we imply also summation over all i and j . Using ellipticity and continuity we have that $\|\mathbf{w}_h\|$ and $\sqrt{\mathbf{w}_h^T \mathbf{A}_h \mathbf{w}_h}$ are equivalent norms for $\mathbf{w}_h \in V_h$ but the constants in the equivalency depend on the material and geometric data [1,3]. Here we note that we use this equivalency only for $\|\mathbf{w}_h\|$ and not for $\|\mathbf{v}_h\|$ in order to be able to directly restate the inf-sup condition in Eq. (8) as

$$\exists \gamma_A > 0 \text{ with } \gamma_h \geq \gamma_A \text{ for all } h \rightarrow 0,$$

$$\gamma_h = \inf_{\mathbf{w}_h \in V_h} \sup_{\mathbf{v}_h \in V_h} \frac{\mathbf{w}_h^T \mathbf{A}_h \mathbf{v}_h}{\sqrt{\mathbf{w}_h^T \mathbf{A}_h \mathbf{w}_h} \sqrt{\mathbf{v}_h^T \mathbf{G}_h \mathbf{v}_h}}, \tag{13}$$

in which γ_h is given by the smallest eigenvalue of the problem $\mathbf{A}_h \mathbf{v}_h = \lambda_k \mathbf{G}_h \mathbf{v}_h \quad \forall \mathbf{v}_h \in V_h.$ (14)

That is, if we denote by $\lambda_1 > 0$ the smallest of the eigenvalues λ_k of this eigenvalue problem, the inf-sup value γ_h of the finite element discretization is given by [1,5,6]

$$\gamma_h = \sqrt{\lambda_1}. \tag{15}$$

To investigate whether $\exists \gamma_A > 0$, we solve Eq. (14) and obtain γ_h using Eq. (15) for a sequence of discretizations of a specific geometry, boundary conditions and material data as the mesh is refined. If the sequence of values γ_h approaches some positive lower bound,

the inf-sup test is passed. However, since the test is here on coercivity, we also want to look at the inf-sup curve, its shape, to identify whether locking is present.

Since the inf-sup expressions in Eqs. (8) and (13) always include the material and geometric data, the smallest eigenvalue λ_1 depends on these data which we need to take into account when we seek to identify from the inf-sup curves whether locking is present.

3. Numerical results

As mentioned above, we use different geometric domains and material conditions to identify whether volumetric, shear, membrane or pinching locking is present and test the standard displacement-based element (H8), the incompatible modes

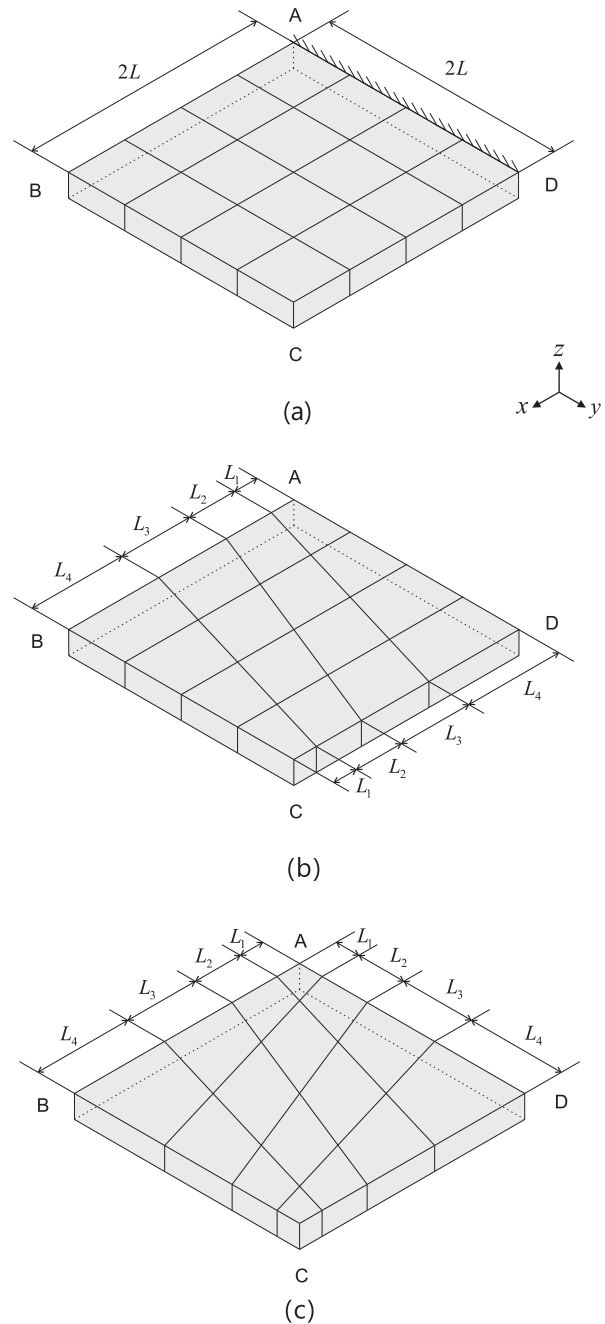


Fig. 6. Cantilever plate (plane strain conditions, $L = 1.0$, $E = 1.0$, and $\nu = 0.3, 0.4$ or 0.499). (a) Problem description with regular mesh (4×4 elements). (b) First type distorted mesh (4×4 elements). (c) Second type distorted mesh (4×4 elements).

element (H8I9), the 3D-MITC8 element and an extension thereof, the 3D-MITC8/s element. The element geometry of these 8-node elements is shown in Fig. 2.

To obtain insight whether volumetric locking is present we use the geometries of Cook's problem, a square cantilever plate, and a square domain with a cavity. In all cases the incompressible limit

is given in plane strain conditions with Poisson's ratio approaching 0.5.

Similarly, to test for possible shear locking, we consider a clamped circular plate, a clamped square plate and a skew plate, where the constraint of zero shear strain is approached by decreasing the plate thickness.

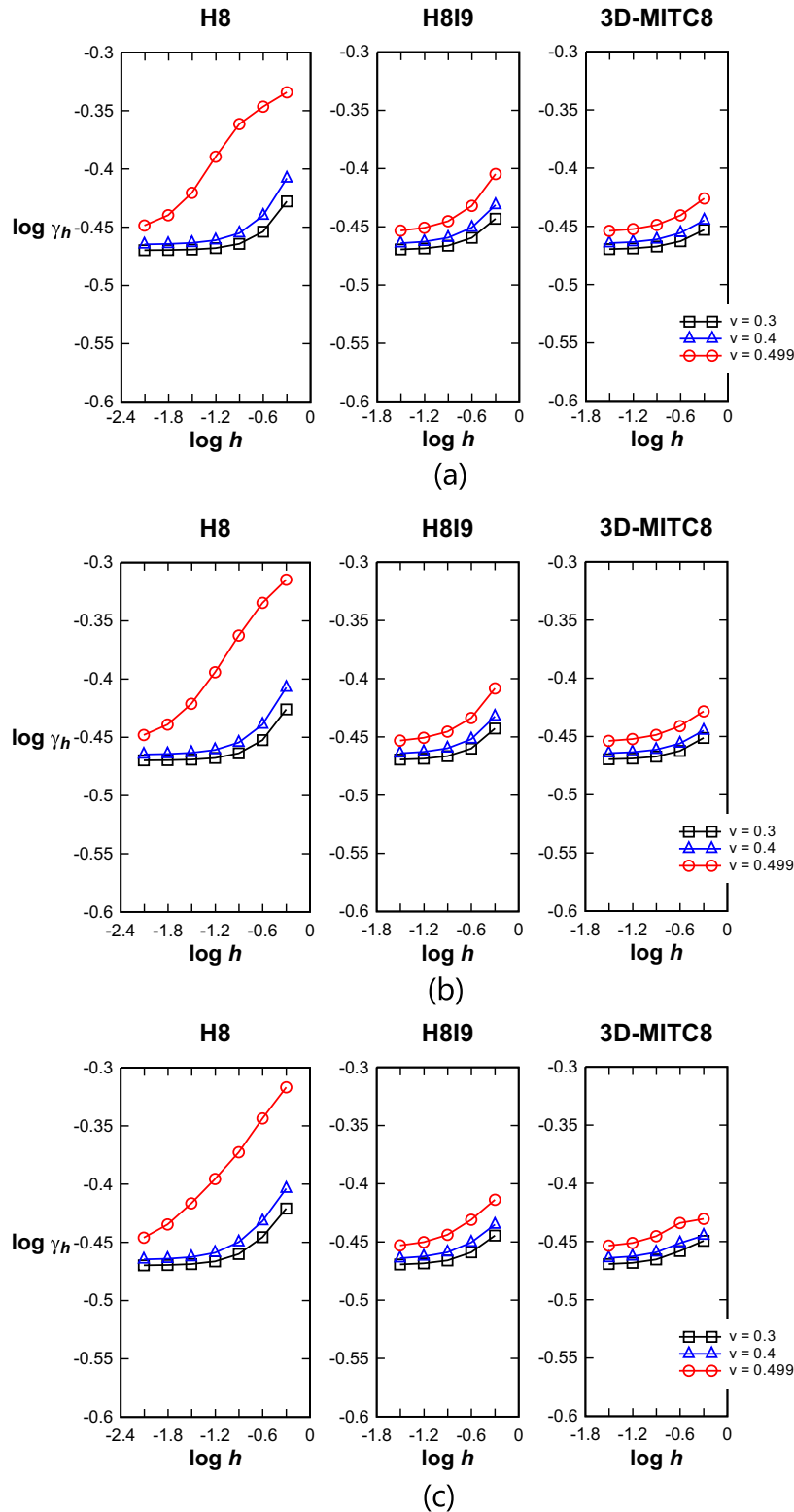


Fig. 7. Inf-sup convergence curves for the cantilever plate using (a) regular meshes, (b) first type distorted meshes and (c) second type distorted meshes.

Finally, to also obtain insight into whether membrane locking is present, we need to consider settings of curved shells and we modify the 3D-MITC8 element formulation so that it is applicable for curved shell analyses. Only a slight modification is needed.

Consider the geometry of the 8-node element shown in Fig. 3. The interpolation is given using the natural coordinates (r, s, t) and we choose (r, s) and (t) corresponding to the in-plane directions and the thickness direction, respectively. We use covariant components of the assumed strain field, with the global Cartesian components of the strain established in the standard way. The 3D-MITC8/s element is obtained from the 3D-MITC8 element formulation by using for the pinching strain (e_{tt}) the nodal point values at the mid-surface [2,19]

$$\tilde{e}_{tt} = \frac{1}{4}(1-r)(1-s)e_{tt}^{(-1,-1,0)} + \frac{1}{4}(1+r)(1-s)e_{tt}^{(1,-1,0)} + \frac{1}{4}(1+r)(1+s)e_{tt}^{(1,1,0)} + \frac{1}{4}(1-r)(1+s)e_{tt}^{(-1,1,0)}. \quad (16)$$

When referring to the 3D-MITC8/s element, the “s” signifies “for shell analysis”.

In the tests, we consider uniform and geometrically distorted meshes to obtain insight into the element behaviors. Since the inf-sup values depend on the material and geometric data, we restrict the test to the practical values of Poisson’s ratio $\nu \leq 0.499$ (to detect volumetric locking) and the ratio of thickness to overall dimension $t/L \geq 1/10,000$ (to detect shear, membrane and pinching locking).

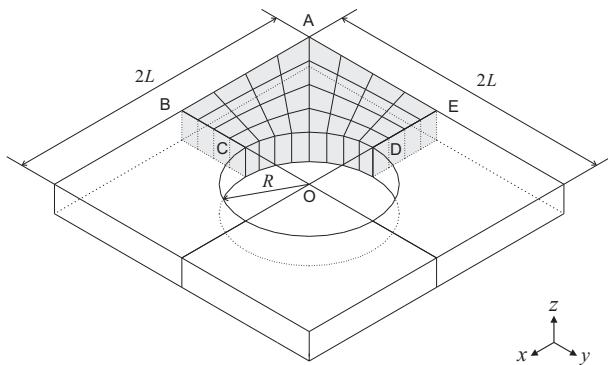


Fig. 8. Square domain with a circular cavity (plane strain conditions, $L = 1.0$, $R = 0.5$, $E = 1.0$, and $\nu = 0.3, 0.4$ or 0.499). The mesh of 4×8 elements is shown.

Considering the three elements that we test, we know of course, based on earlier experiences, that the H8 element locks, the H819 element performs in general better than the H8 element, and we know that the 3D-MITC8 element performs in some analyses even better than the H819 element [15]. Therefore, for the purpose of gaining insight, we also endeavor to relate the results given in Ref. [15] to the results obtained here in the inf-sup testing.

An inherent disadvantage of a numerical test versus an analytical proof is that the test can only be performed to a certain mesh size (a small value of element size h). In practical analyses, of course, meshes are only refined up to a limit of element size. We used this fact to guide us in decreasing the element sizes to reasonable practical values in the tests (hence we cannot give conclusions on solutions of inf-sup values for even smaller values of h).

3.1. Locking in the analysis of incompressible media

In this section we focus on identifying locking in the analysis of incompressible media.

3.1.1. Cook’s cantilever

We consider the geometry and boundary conditions of Cook’s cantilever shown in Fig. 4 [15,25]. The cantilever is clamped at one end. We consider the solutions using plane strain conditions with $\nu = 0.3, 0.4$ and 0.499 , and meshes of $N \times N$ elements with $N = 2, 4, 8, 16$ and 32 . The plane strain condition is modeled by imposing $u_z = 0$ for the entire mesh.

Fig. 5 shows the convergence of the inf-sup values as a function of the element size $h = 1/N$. For $\nu = 0.499$, the inf-sup values using the H8 element are large for coarse meshes. On the other hand, the inf-sup values using the 3D-MITC8 and H819 elements are much less dependent on Poisson’s ratio, and specifically for the coarse meshes used.

The large inf-sup values of the meshes of the H8 element are due to the fact that the element is very stiff when $\nu = 0.499$ and indicate the locking behavior seen in the actual solution of Cook’s problem [15]. Hence the inf-sup curves given here correspond quite well to the convergence curves given in Ref. [15].

3.1.2. Cantilever plate in plane strain conditions

We consider the cantilever square plate shown in Fig. 6 and assume plane strain conditions with Poisson’s ratios $\nu = 0.3, 0.4$ and 0.499 [15]. For the solutions, we use regular and two types of distorted meshes with $N \times N$ elements, $N = 2, 4, 8, 16$ and 32 , see Fig. 6(a), (b) and (c), where the element edges are discretized in the ratio $L_1:L_2:L_3: \dots L_N = 1:2:3: \dots N$.

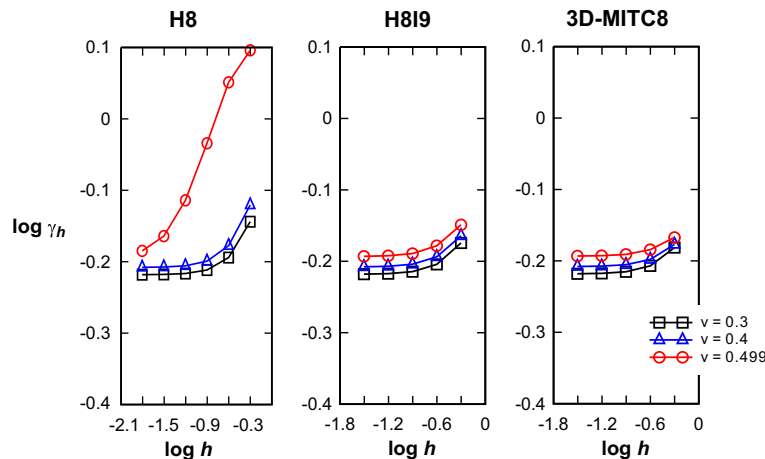


Fig. 9. Inf-sup convergence curves for the square domain with a cavity.

The following boundary conditions are imposed: $u_x = u_y = u_z = 0$ along AD, and $u_z = 0$ for the entire mesh. The element size is $h = 1/N$.

Fig. 7 shows the convergence of the inf-sup values, and we note that the values are well bounded for the 3D-MITC8 and H8I9 elements using the uniform and distorted meshes. The observations and conclusions given in Section 3.1.1 are here also applicable, and once again the inf-sup curves correspond quite well to the convergence curves obtained in the solutions given in Ref. [15].

3.1.3. Square domain with a circular cavity

We consider a square structural domain with a circular cavity as shown in Fig. 8 [15]. Plane strain conditions are assumed with Poisson’s ratios $\nu = 0.3, 0.4$ and 0.499 . Because of symmetry, only one-quarter of the structure is modeled using $N \times 2N$ elements with $N = 2, 4, 8, 16$ and 32 . The following boundary conditions are imposed: $u_x = 0$ along BC, $u_y = 0$ along DE, and $u_z = 0$ for the entire mesh. The element size is $h = 1/N$.

Fig. 9 shows the convergence of the inf-sup values. Considering the almost incompressible conditions, we only see for the inf-sup values using the H8I9 and 3D-MITC8 elements well-bounded convergence. Again, the observations and conclusions given in Section 3.1.1 are here too applicable, and the inf-sup curves correspond to the convergence curves given in Ref. [15].

3.2. Shear locking

In this section we focus on identifying shear locking in the element formulations by plotting the inf-sup values for various thickness to length ratios of plates.

3.2.1. Clamped circular plate

To test for shear locking, we consider a circular plate clamped along its perimeter, see Fig. 10. Utilizing symmetry, we model only one quarter of the plate using N elements per radius ($N/2 \times N/2 \times 3$ elements) with $N = 4, 8, 16, 32$ and 64 . We vary the ratio of the thickness to the overall dimension of the structure, $t/L = 1/10, 1/100, 1/1000$ and $1/10,000$. The element size is $h = L/N$. The boundary conditions are $u_x = 0$ along BC, $u_y = 0$ along AC and $u_x = u_y = u_z = 0$ along AB. We use only one layer of elements in the thickness direction.

Fig. 11 shows the convergence of the inf-sup values as a function of the element size $h = 1/N$. For plates with $t/L = 1/100$ or

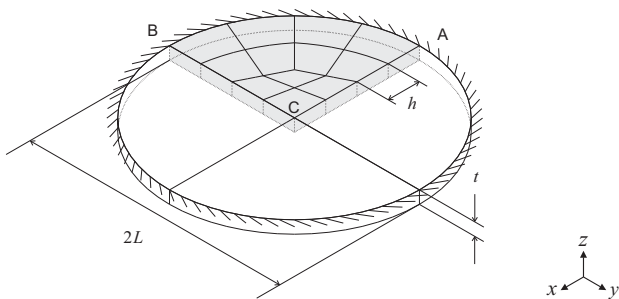


Fig. 10. Clamped circular plate ($L = 1.0, t = 1/10, 1/100, 1/1000$ or $1/10000, E = 1.0$ and $\nu = 0.0$). The mesh with 4 elements per sides is shown.

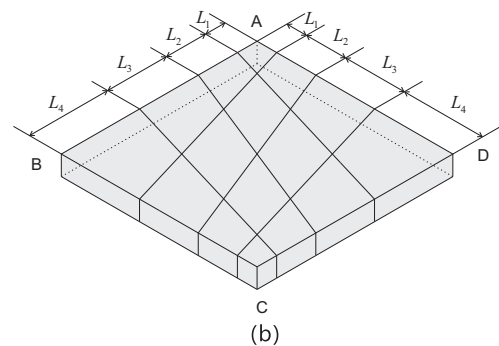
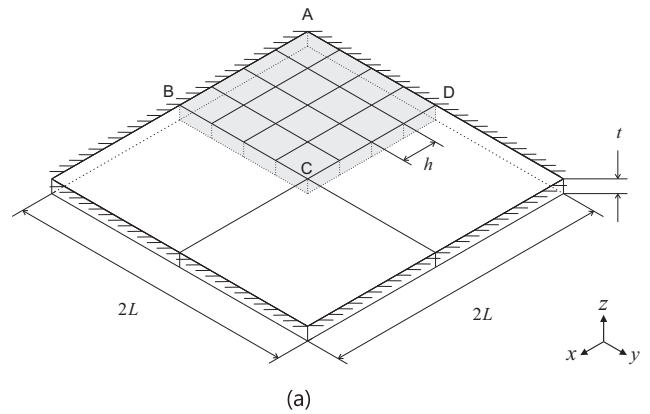


Fig. 12. Clamped square plate ($L = 1.0, t = 1/10, 1/100, 1/1000$ or $1/10000, E = 1.0$ and $\nu = 0.0$). (a) Problem description with regular mesh (4×4 elements). (b) Distorted mesh (4×4 elements).

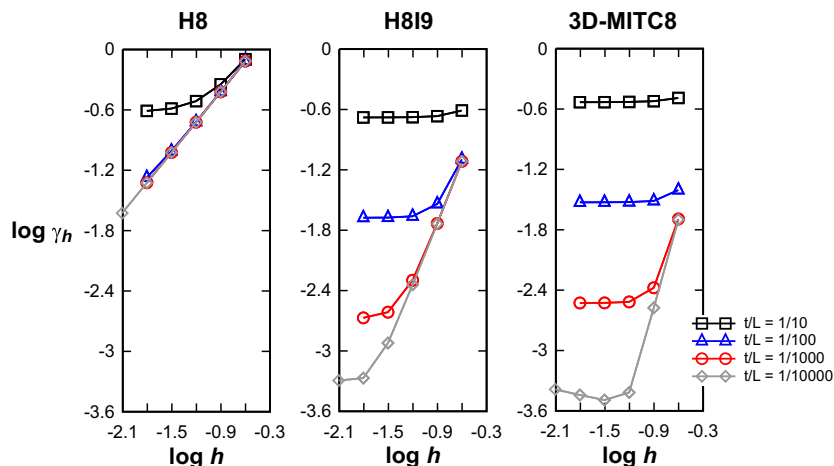


Fig. 11. Inf-sup convergence curves for the clamped circular plate.

thinner, the inf-sup values using the H8 element continue to decrease (for the meshes used), the H819 element shows a good behavior for the case of thick plates, whereas the inf-sup values using the 3D-MITC8 element are bounded for all thickness values considered.

It is interesting to note that the inf-sup values using the H8 element are much larger than those employing the other elements because the H8 element is stiffer (see the observations discussed in Section 3.1.1). Also, the inf-sup values using the H819 and 3D-MITC8 elements in coarse meshes are large because the discretizations are stiff when h is large.

We further note that using the 3D-MITC8 element, the inf-sup values at small h decrease by about an order of magnitude as t/L decreases by the same order, which is due to the norms used.

The above observations are also applicable for the inf-sup value results given below.

3.2.2. Clamped square plate

We consider a square plate clamped along its all four sides, see Fig. 12(a) [15]. Utilizing symmetry, only one quarter of the plate is modeled using $N \times N$ elements with $N = 4, 8, 16, 32$ and 64 . Four ratios of the thickness to the overall dimension of the structure are considered, $t/L = 1/10, 1/100, 1/1000$ and $1/10,000$. The element size is $h = L/N$. The boundary conditions are $u_x = 0$ along BC, $u_y = 0$ along DC and $u_x = u_y = u_z = 0$ along AB and AD. We use only one layer of elements in the thickness direction.

We also perform the convergence studies with the distorted mesh patterns shown in Fig. 12(b), in which each edge is discretized by the elements in the following ratio: $L_1:L_2:L_3: \dots L_N = 1:2:3: \dots N$ for the $N \times N$ element mesh.

Fig. 13 shows the convergence of the inf-sup values for the regular and distorted mesh cases. For the distorted meshes used, we find that only the inf-sup values using the 3D-MITC8 element behave well for all t/L ratios. This corresponds to the observation that, in general, 3D solid elements do not perform well in plate bending analyses and the convergence deteriorates with mesh distortions [15].

We also note that these inf-sup curves correspond quite well to the convergence curves given in Ref. [15].

3.2.3. Clamped skew plate

We consider the skew plate shown in Fig. 14. The plate is modeled using $N \times N$ elements with $N = 4, 8, 16, 32$ and 64 . We are interested in investigating the effect of the skew distortion of the plate, and hence consider the cases of skew angles $\theta = 60^\circ$ and $\theta = 30^\circ$. The thickness to the overall dimension of the structure considered is $t/L = 1/10, 1/100, 1/1000$ and $1/10,000$. The element size is $h = L/N$. The clamped boundary condition $u_x = u_y = u_z = 0$ is used along AB, BC, CD and AD, and we use only one layer of elements in the thickness direction.

Fig. 15 shows that as the thickness becomes small, the inf-sup values using the H8 and H819 elements decrease continuously

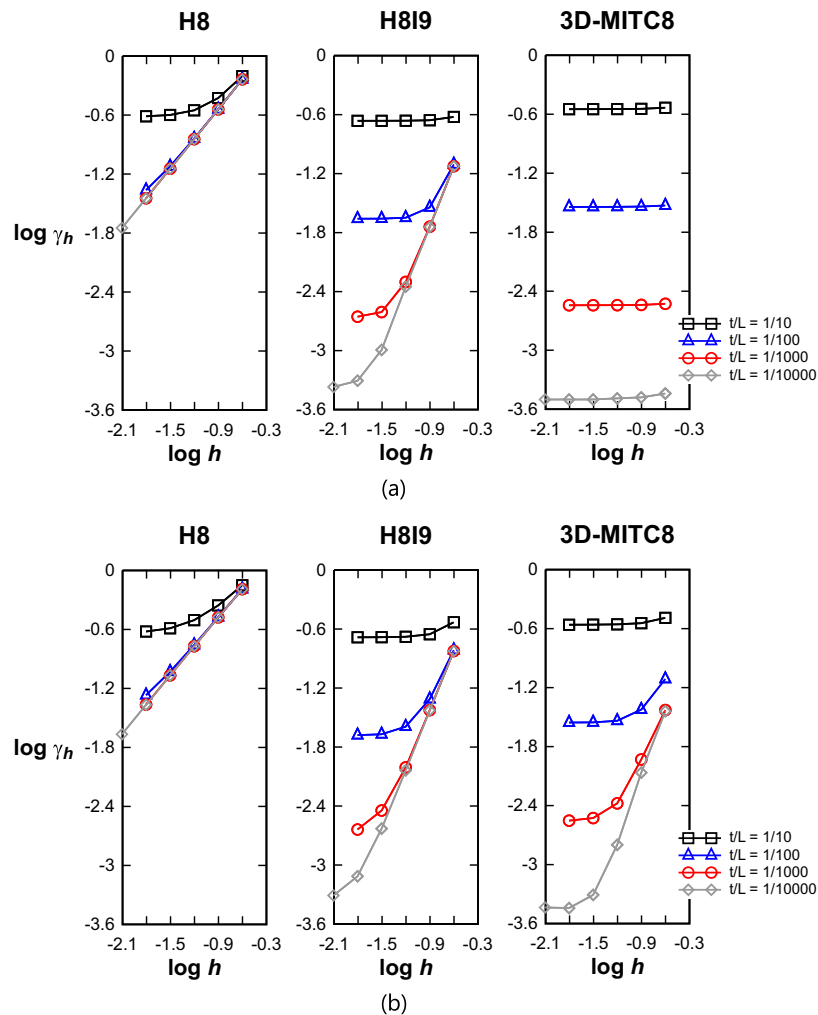


Fig. 13. Inf-sup convergence curves for the clamped square plate using (a) regular and (b) distorted meshes.

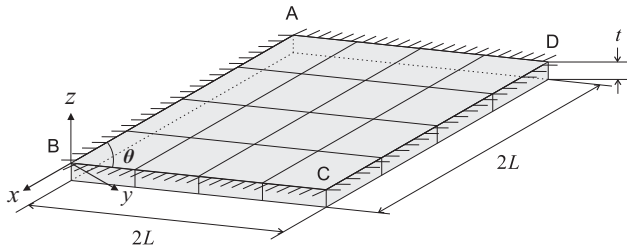


Fig. 14. Skew plate ($L = 1.0$, $t = 1/10, 1/100, 1/1000$ or $1/10000$, $E = 1.0$ and $\nu = 0.0$). Geometry and mesh of 4×4 elements.

(for the meshes used) while the inf-sup values using the 3D-MITC8 element converge to a positive asymptotic bound, even already for a few mesh refinements regardless of the plate geometry or thickness. Hence only the 3D-MITC8 element passes this test for all t/L ratios.

3.3. Shear, membrane and pinching locking

Shear and membrane locking effects can occur when low-order elements are used in the analysis of curved shell geometries, in particular when distorted meshes are employed. The effect of pinching locking can also be seen in the analysis of shells. We consider here two shell geometries for the inf-sup test.

3.3.1. Cylindrical shell geometry

We consider the cylindrical shell geometry shown in Fig. 16(a) [2]. In addition to identifying possible shear locking, we are interested in possible membrane locking effects due to 3D mesh distortions in an analysis of the curved shell and in pinching locking. Utilizing symmetry, only one-eighth of the cylinder is modeled using $N \times N$ elements with $N = 4, 8, 16, 32$ and 64 . The ratios of thickness to overall dimension of the structure considered are $t/L = 1/10, 1/100, 1/1000$ and $1/10,000$. The element size is $h = L/N$. The structural model is free on the edge AD, $u_z = 0$ along AB, $u_y = 0$ along DC, and $u_x = 0$ along BC. We use only one layer of elements in the thickness direction.

When using the regular mesh in Fig. 16(a), the mesh near the free end is graded with a boundary layer of width $0.5\sqrt{t}$ [2]. We also perform the convergence studies with the distorted mesh shown in Fig. 16(b).

Fig. 17 shows the convergence of the inf-sup values. Due to the effects of shear, membrane and pinching locking, the inf-sup values using the H8 element are not yet bounded (for the meshes used) and the values using the H8I9 element are also not yet showing a clear bound in the case of small shell thickness and using the distorted meshes. Here only the 3D-MITC8 and the 3D-MITC8/s elements show a good behavior, with the 3D-MITC8/s element performing best. The curves indicate that there is some pinching locking in the 3D-MITC8 element which has been remedied by

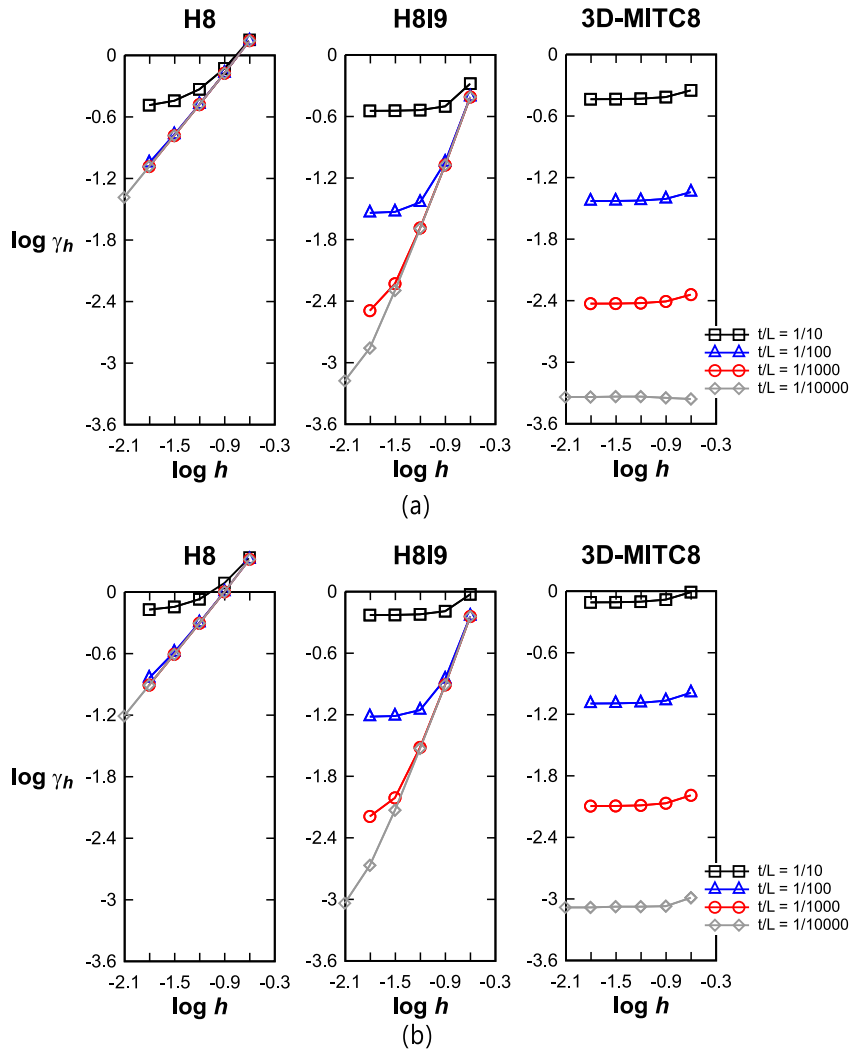


Fig. 15. Inf-sup convergence curves for the skew plate with (a) moderate skew ($\theta = 60^\circ$) and (b) high skew ($\theta = 30^\circ$).

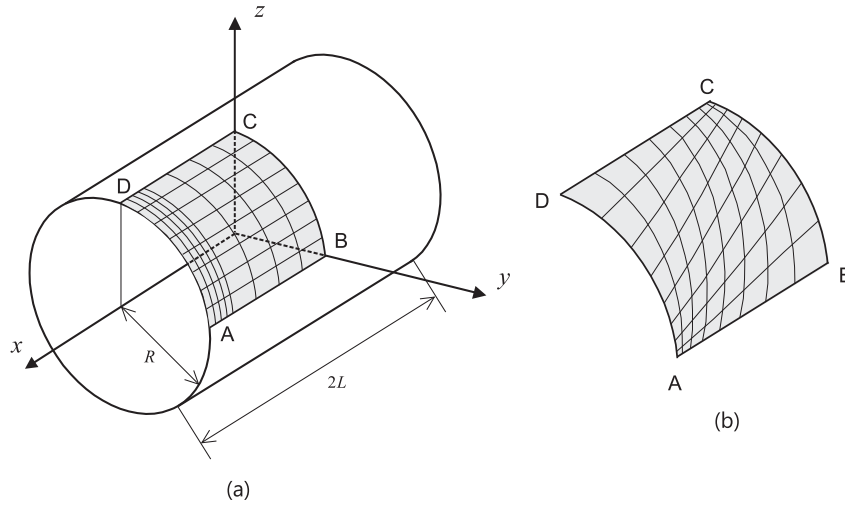


Fig. 16. Cylindrical shell ($L = R = 1.0$, $t = 1/10, 1/100, 1/1000$ or $1/10000$, $E = 1.0$ and $\nu = 0.0$). (a) Geometry with the graded regular mesh (8×8 elements). (b) The distorted mesh of Fig. 12(b) (8×8 elements).

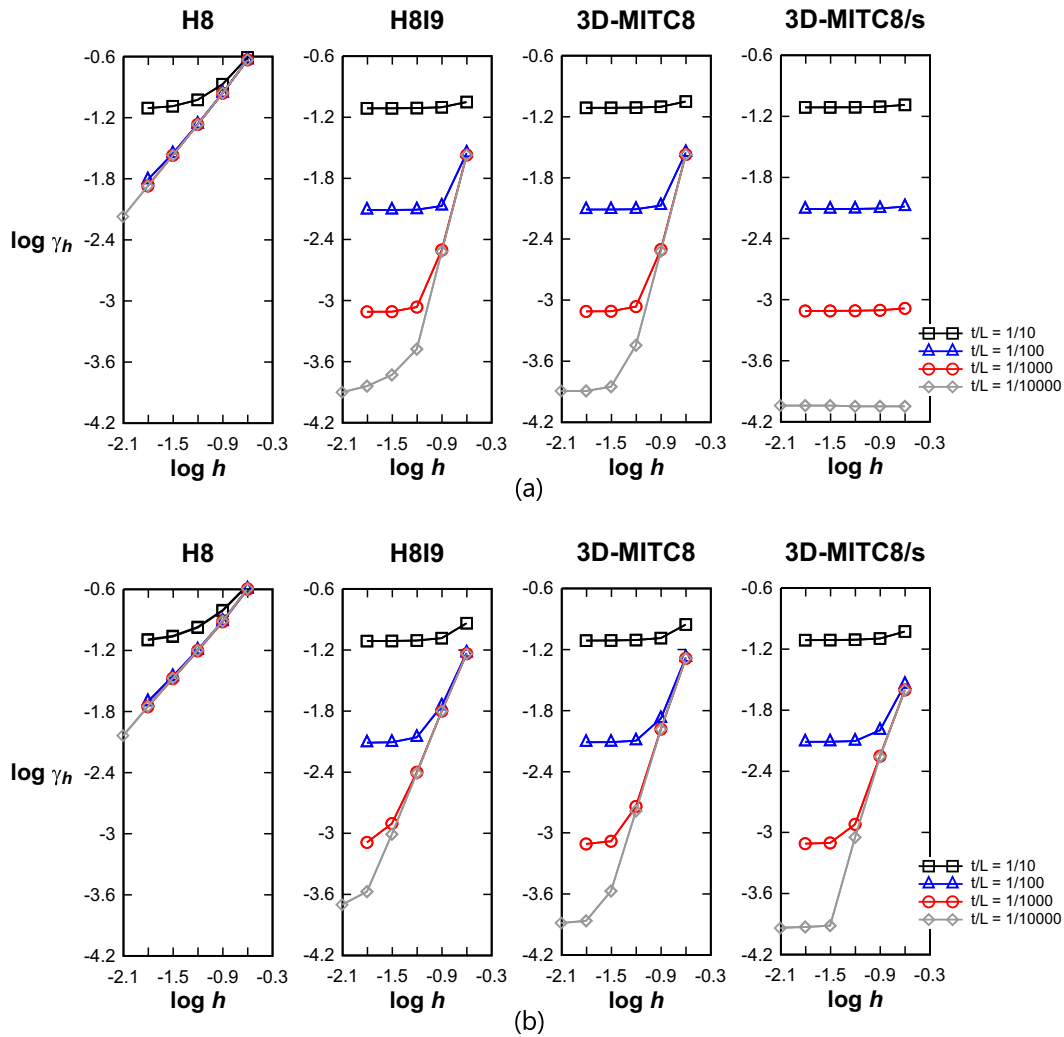


Fig. 17. Inf-sup convergence curves for the cylindrical shell using (a) graded regular and (b) distorted meshes.

the interpolation of Eq. (16). When comparing the curves in Fig. 17 (a) and Fig. 17(b) we need to keep in mind that the boundary layer is not modeled when a distorted mesh is used.

3.3.2. Hyperboloidal shell

We consider the doubly curved hyperboloidal shell shown in Fig. 18(a) [2,25]. The mid-surface of the shell structure is given by

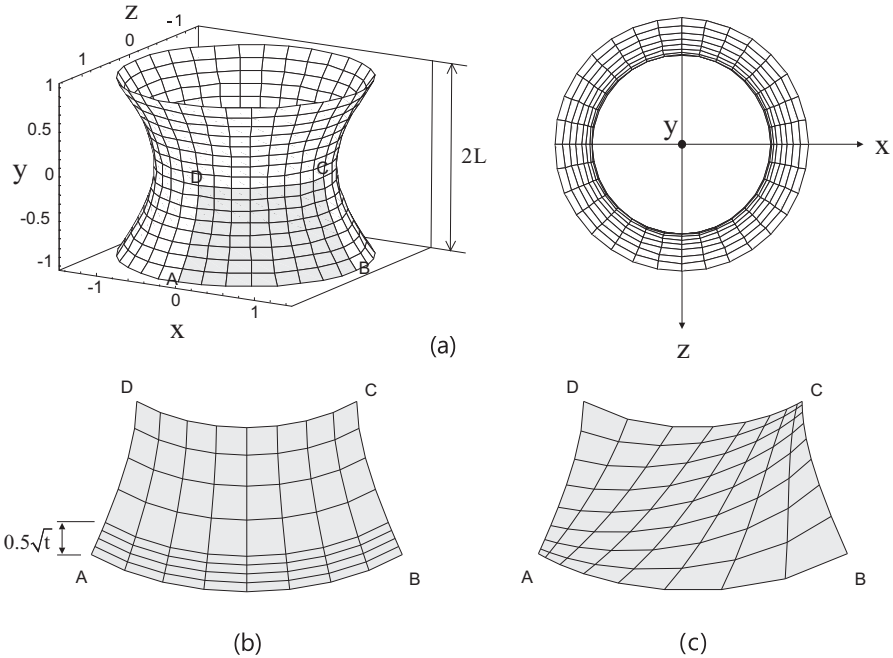


Fig. 18. Hyperboloid shell ($L = 1.0$, $t = 1/10, 1/100, 1/1000$ or $1/10000$, $E = 1.0$ and $\nu = 0.0$). (a) Geometry description. (b) Graded regular mesh (8×8 elements). (c) The distorted mesh of Fig. 12(b) (8×8 elements).

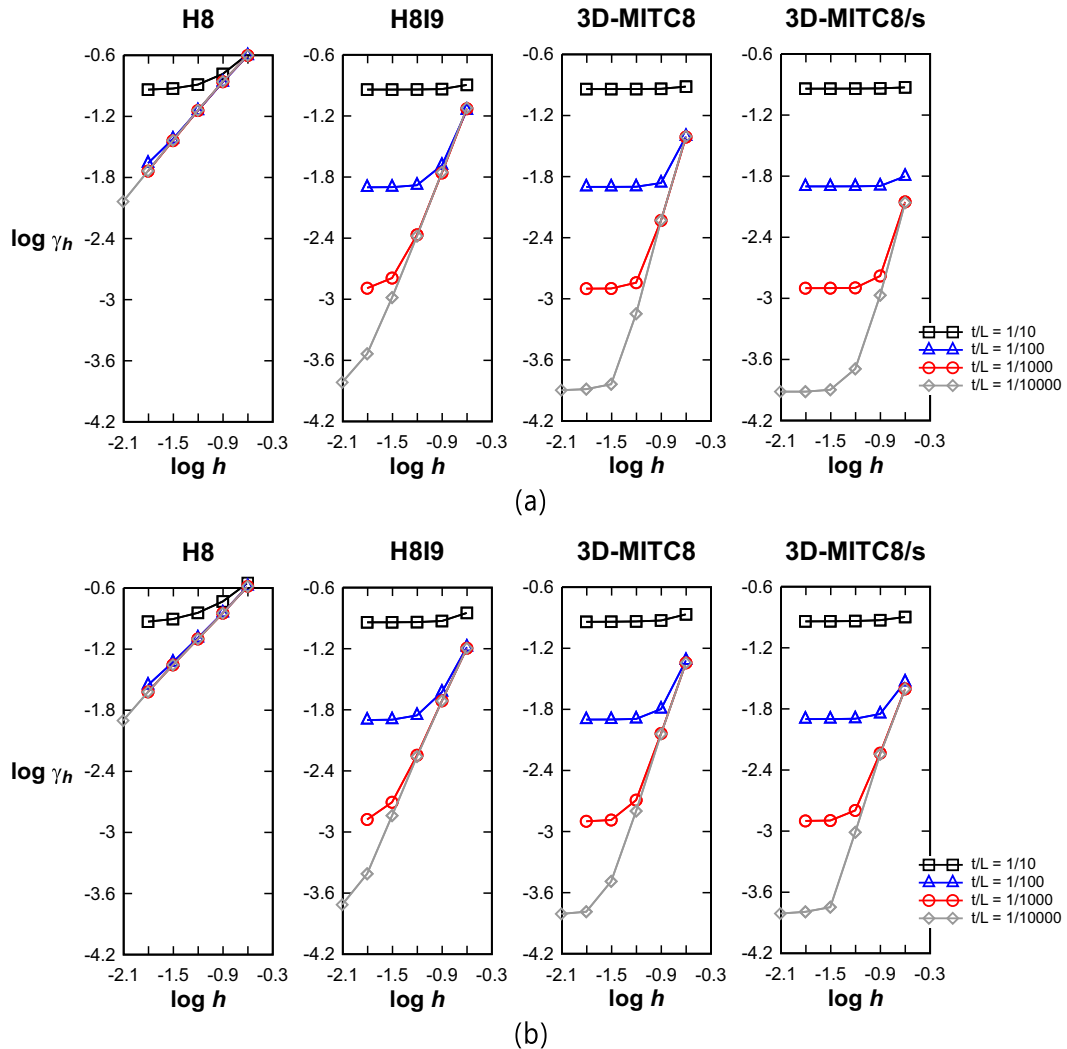


Fig. 19. Inf-sup convergence curves for the hyperboloid shell using (a) graded regular and (b) distorted meshes.

$$x^2 + z^2 = 1 + y^2; \quad y \in [-1, 1]. \quad (17)$$

Utilizing symmetry, only one-eighth of the structure is modeled using $N \times N$ elements with $N = 4, 8, 16, 32$ and 64 . As thickness to length ratios we consider $t/L = 1/10, 1/100, 1/1000$ and $1/10,000$. The element size is $h = L/N$. The structural model is free at the edge AB, $u_z = 0$ along BC, $u_x = 0$ along AD, and $u_y = 0$ along DC. We use only one layer of elements in the thickness direction.

When using the regular mesh in Fig. 18(b), the mesh near the free end is graded with a boundary layer of width $0.5\sqrt{t}$ [2]. We also perform the convergence studies with the distorted meshes shown in Fig. 18(c).

Fig. 19 shows the convergence of the inf-sup values. Due to the combined effects of locking, the inf-sup values using the H8 and H819 elements continue to decrease (for the meshes used) when the shell thickness is small, whereas the results for the 3D-MITC8 and 3D-MITC8/s elements show that a lower limit is reached for all t/L ratios. Hence the same conclusions as in Section 3.3.1 are valid, that is, only these two elements perform quite well when considering a small shell thickness, and the 3D-MITC8/s element performs best. This solution shows that for thin shell structures, clearly the use of a shell element is preferable [25].

As in Section 3.3.1, when comparing the curves in the figures we need to keep in mind that the boundary layer is not modeled when a distorted mesh is used.

3.4. Initially compressed block problem

Finally, we turn to considering geometric nonlinear effects in one simple problem. We consider the long block shown in Fig. 20 (a). Plane strain conditions are assumed in the x -direction with

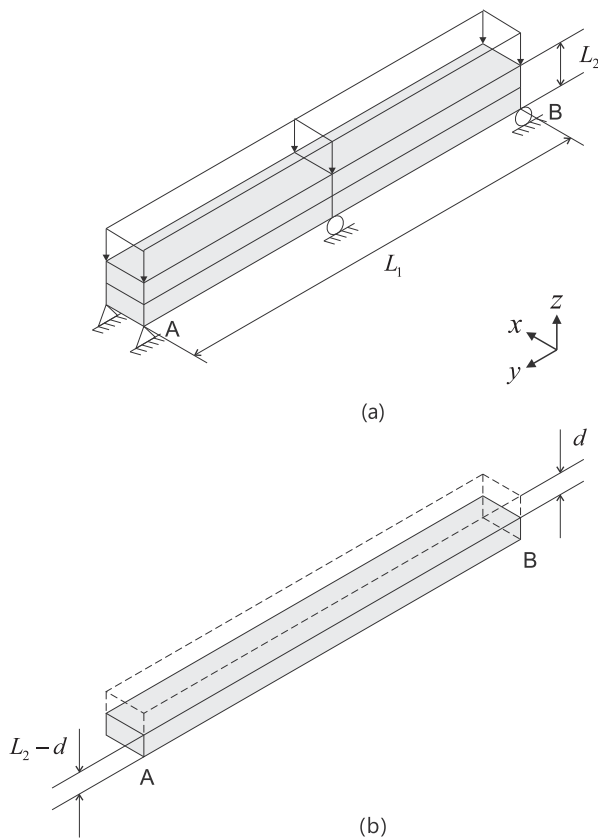


Fig. 20. Initially compressed block (plane strain conditions, $L_1 = 10.0$, $L_2 = 1.0$, $E = 1.0$ and $\nu = 0.0$). (a) Problem description in initial configuration (mesh of 2×2 elements). (b) Current deformed configuration.

Poisson's ratio $\nu = 0.0$. The block is subjected to an initial compressive displacement in the z -direction, see Fig. 20(b). The purpose is to investigate the behavior of the inf-sup value near the critical volumetric strain identified by Sussman and Bathe for the incompatible modes element [24]. Noting that a positive value of the inf-sup expression pertains to the stability of the solution, we

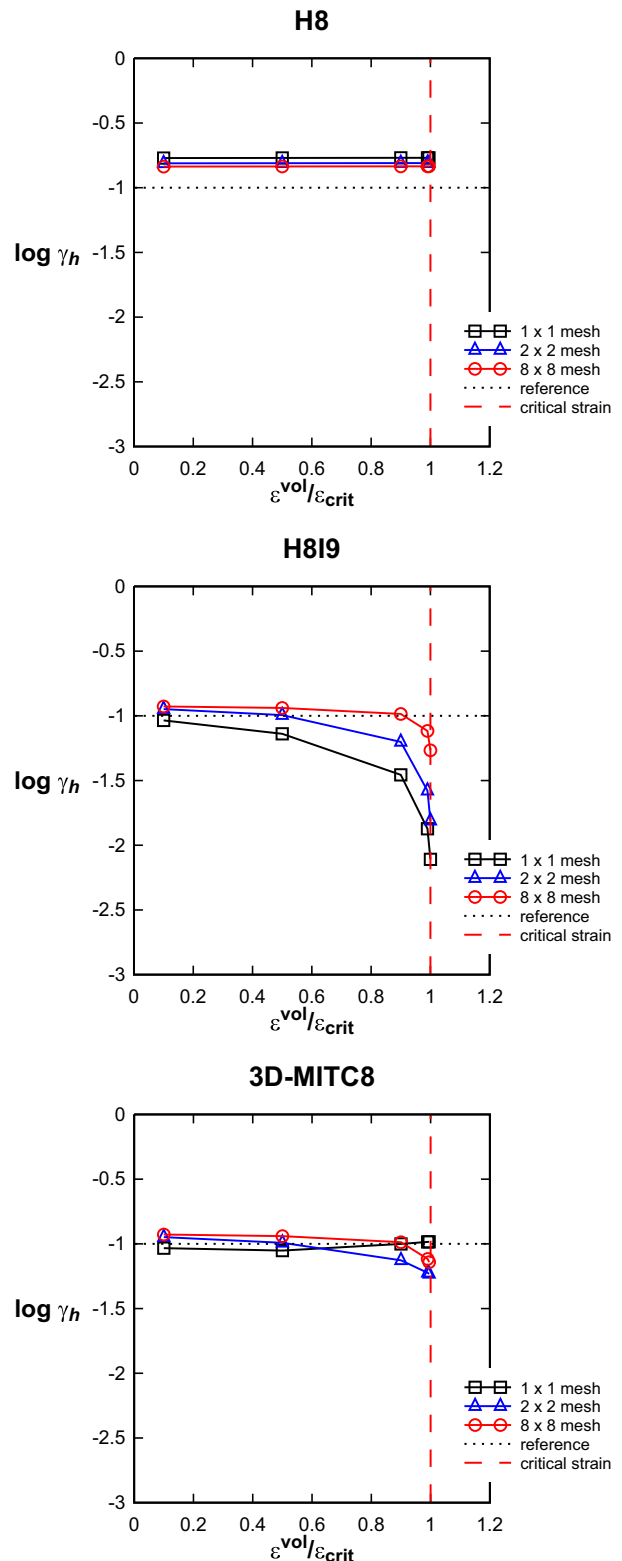


Fig. 21. Inf-sup values for the initially compressed block.

increase the volumetric strain and investigate if the inf-sup values decrease asymptotically at the spurious critical strain limit. The structure is modeled using $N \times N$ elements with $N = 1, 2$ and 8 corresponding to the z and y -directions, see Fig. 20(b). The element size is $h = 1/N$.

The vertical displacement $u_z = -d$ is prescribed giving $\varepsilon^{vol} = \varepsilon_{zz} = -d/L_2$. Ref. [24] gives that an H819 element in nonlinear analysis will undergo a spurious mechanism at the critical strain $\varepsilon^{vol} = \varepsilon_{crit} = -(L_2/L_1)^2$. We perform the inf-sup test with the tangent stiffness matrix at the deformed configuration in Fig. 20(b) to see whether a spurious instability occurs.

Fig. 21 shows the convergence of the inf-sup values. We note the reference value $\gamma_h = 10^{-1}$ is obtained with a linear stiffness matrix not including the initial compression. The inf-sup values using the H8 element are slightly higher but are constant indicating, as expected, a very stable behavior. Inf-sup values close to the reference value are obtained for the 3D-MITC8 and H819 elements if the compression is small. However, as the imposed volumetric strain approaches the limit of spurious buckling, the inf-sup values using the H819 element sharply decrease. The inf-sup values employing the 3D-MITC8 element also decrease as the compression is increased but remain greater than zero at the spurious critical strain for the incompatible modes element. Hence the coercivity of the 3D-MITC8 element discretization is preserved.

These observations correspond to the experiences reported in Refs. [15,24].

4. Conclusions

Our objective in this paper was to obtain further insight into the reliability of 8-node hexahedral elements using inf-sup tests. We considered the standard 8-node displacement-based element, the 8-node element with incompatible modes and the recently proposed 3D-MITC8 element. Our focus was on whether these elements lock in the analyses of (almost) incompressible media (volumetric locking), and in the analyses of plates (shear locking) and shells (shear, membrane and pinching locking).

Since the mathematical theory of the 3D-MITC8 element needs to first be developed for a thorough analytical investigation, we used a simple but quite general approach to obtain some insight into the various locking behaviors of the elements. Namely, we used the inf-sup condition on the complete matrix described by displacement degrees of freedom only and considered various geometries, boundary conditions, material properties and thicknesses to see the behaviors of the inf-sup values as the meshes are refined. The inf-sup expression is in fact evaluating whether coercivity is satisfied but by studying the inf-sup curves we can obtain some insight into the locking behaviors of the elements. Indeed, we saw that the calculated inf-sup curves correspond well to the convergence curves obtained for the elements in Ref. [15].

As expected we could read from the inf-sup curves that the H8 element is locking in all cases considered. In the analysis of incompressible media, the H819 and 3D-MITC8 elements show a similar performance, but in the analysis of plates considering shear locking the 3D-MITC8 element performs best. For the analysis of shells, the H819 and 3D-MITC8 elements behave similarly when considering moderately thick shells, for thin shells the 3D-MITC8 element might be used but the 3D-MITC8/s element performs best.

In addition, we applied the inf-sup test in a geometrically nonlinear state of an initially compressed block and saw that the 3D-MITC8 element displayed stability unlike the H819 element. However, more research for such nonlinear conditions is needed.

While the results given in the paper are valuable in providing novel insight into the behavior of the elements tested, considering the 3D-MITC8 element, clearly a thorough mathematical analysis is very desirable. Such analysis may also identify more effective inf-sup tests.

Acknowledgement

We would like to thank Dominique Chapelle of Inria, France, for valuable discussions on this paper.

References

- [1] Bathe KJ. Finite element procedures. Prentice Hall; 1996, 2nd ed. Bathe KJ, Watertown, MA; 2014 and Higher Education Press, China; 2016.
- [2] Chapelle D, Bathe KJ. The finite element analysis of shells – fundamentals. 2nd ed. Berlin: Springer-Verlag; 2011.
- [3] Brezzi F, Bathe KJ. A discourse on the stability conditions for mixed finite element formulations. *Comput Math Appl Mech Eng* 1990;82(1-3):27–57.
- [4] Brezzi F, Fortin M. Mixed and hybrid finite element methods. New York: Springer-Verlag; 1991.
- [5] Chapelle D, Bathe KJ. The inf-sup test. *Comput Struct* 1993;47(4-5):537–45.
- [6] Bathe KJ. The inf-sup condition and its evaluation for mixed finite element methods. *Comput Struct* 2001;79:243–52. 971.
- [7] Pantuso D, Bathe KJ. A four-node quadrilateral mixed-interpolated element for solids and fluids. *Math Mod Meth Appl Sci* 1995;5(8):1113–28.
- [8] Wang X, Bathe KJ. On mixed elements for acoustic fluid structure interactions. *Math Mod Meth Appl Sci* 1997;7(3):329–43.
- [9] Bathe KJ, Hendriana D, Brezzi F, Sangalli G. Inf-sup testing of upwind methods. *Int J Num Meth Eng* 2000;48:745–60.
- [10] Nissen K, Wall WA. Pressure-stabilized maximum-entropy methods for incompressible Stokes. *Int J Num Meth Fluid* 2016;82:35–56.
- [11] Nodargi NA, Bisegna P. A novel high-performance mixed membrane finite element for the analysis of inelastic structures. *Comput Struct* 2017;182:337–53.
- [12] Na S, Sun W. Computational thermo-hydro-mechanics for multiphase freezing and thawing porous media in the finite deformation range. *Comp Meth Appl Mech Eng* 2017;318:667–700.
- [13] Duboeuf F, Béchet E. Embedded solids of any dimension in the X-FEM. Part II – Imposing Dirichlet boundary conditions. *Finit Elem Anal Des* 2017;128:32–50.
- [14] Dortdivanlioglu B, Krischok A, Beirão da Veiga L, Linder C. Mixed isogeometric analysis of strongly coupled diffusion in porous materials. *Int J Num Meth Eng* 2018;114(1):28–46.
- [15] Ko Y, Bathe KJ. A new 8-node element for analysis of three-dimensional solids. *Comput Struct* 2018;202:85–104.
- [16] Wilson EL, Ibrahimbegovic A. Use of incompatible displacement modes for the calculation of element stiffnesses or stresses. *Finit Elem Anal Des* 1990;7(3):229–41.
- [17] Iosilevich A, Bathe KJ, Brezzi F. On evaluating the inf-sup condition for plate bending elements. *Int J Num Meth Eng* 1997;40(19):3639–63.
- [18] Bathe KJ, Iosilevich A, Chapelle D. An inf-sup test for shell finite elements. *Comput Struct* 2000;75(5):439–56.
- [19] Chapelle D, Ferent A, Le Tallec P. The treatment of “pinching locking” in 3D-shell elements. *M2AN Math Model Num Anal* 2003;37(1):143–58.
- [20] Chapelle D, Bathe KJ. On the ellipticity condition for model-parameter dependent mixed formulations. *Comput Struct* 2010;88:581–7.
- [21] Wriggers P, Reese S. A note on enhanced strain methods for large deformations. *Comp Meth Appl Mech Eng* 1996;135(3-4):201–9.
- [22] Pantuso D, Bathe KJ. On the stability of mixed finite elements in large strain analysis of incompressible solids. *Finit Elem Anal Des* 1997;28(2):83–104.
- [23] Wall WA, Bischoff M, Ramm E. A deformation dependent stabilization technique, exemplified by EAS elements at large strains. *Comp Meth Appl Mech Eng* 2000;188(4):859–71.
- [24] Sussman T, Bathe KJ. Spurious modes in geometrically nonlinear small displacement finite elements with incompatible modes. *Comput Struct* 2014;140:14–22.
- [25] Ko Y, Lee PS, Bathe KJ. A new 4-node MITC element for analysis of two-dimensional solids and its formulation in a shell element. *Comput Struct* 2017;192:34–49.